Electrical characterization of an inductively coupled gaseous electronics conference reference cell

Electrical characterization of an inductively coupled gaseous electronics conference reference cell

S. V. Singh[1,a] and C. Pargmann[2]
[1]*Department of Applied Physics, Eindhoven University of Technology, P.O. Box 513, 5600 MB Eindhoven, The Netherlands*
[2]*German Aerospace Center, Institute of Technical Physics, Langer Grund, D-74239 Hardthausen, Germany*

(Received 2 May 2008; accepted 2 September 2008; published online 24 October 2008)

Plasma parameters and particularly the external electrical operational parameters are examined with respect to mode transition and hysteresis. The external electrical parameters such as antenna current (I_c) and antenna voltage (V_c) amplitudes are measured after the matching network and discussed for an inductively coupled argon discharge. A wide range of discharge conditions by varying applied power (up to 150 W at 13.56 MHz), gas pressure (0.7–7.5 Pa), and electrostatic coupling strength are measured for a gaseous electronics conference radio frequency reference cell. The effect on the power coupling efficiency by varying electrostatic coupling strength is studied via implementing two distinct grounded Faraday shields, in addition to the original nonshielded condition. A brief discussion on the evolution of floating potential, plasma potential, electron density, and electron energy distribution function with power and pressure is also presented mainly in context to mode transitions and hysteresis. Relatively smooth transitions in the plasma parameters and in the external electrical parameters are measured close to *H* to *E* mode transition region. Contrary to plasma parameters, however, the reverse transition from *E* to *H* mode was found to be abrupt in external parameters. The plasma parameters are measured using a commercial Langmuir probe, whereas the antenna currents and voltages are measured using a homebuilt Rogowski coil and capacitor divider, respectively. © *2008 American Institute of Physics*. [DOI: 10.1063/1.3000667]

I. INTRODUCTION

Inductively coupled radio frequency (rf) discharges have a long history and have been rigorously used for the understanding of low temperature plasmas. In the recent years, inductively coupled plasmas (ICPs) have been intensively used for plasma processing and light source technology. They are basically electrodeless and are capable of providing high plasma densities at low pressures (even below 1 Pa).[1,2] The ICPs have low ion energy and minimal power loss in the sheath.[3] These features have stimulated research activities on the basic plasma phenomena occurring in such discharges. A distinct feature of an ICP is the existence of two operational modes which dramatically differ in their electrical and plasma properties.[1–5] The so-called *E* mode excites at low rf powers and exhibits a faint light emission, a relatively low electron density ($\sim 10^9$ cm^{-3}), a high electron mean energy, and a high plasma and floating potential. It is thought to be maintained by the electrostatic field developed across the powered end of the coil and the ground and, therefore, often referred to as capacitive mode. On the other hand, the so-called *H* mode which excites at high rf powers is characterized by a bright light emission, a high electron density (exceeding 10^{11} cm^{-3}), a relatively low electron mean energy, and a low plasma and floating potential. It is believed to be maintained by the azimuthal electric field induced by the rf antenna current (I_c) and is often referred to as inductive mode. Abrupt as well as almost smooth transitions between the two modes are reported by several authors.[3–7] In addition, hysteresis effects were observed meaning that the transition from the *E* mode to the *H* mode occurs under different conditions, e.g., electron density, supplied power [antenna current and antenna voltage (V_c)] than the reverse transition from the *H* mode to the *E* mode.[2,7,8]

Several attempts have been made to measure the electrical and plasma characteristics of inductive discharges.[7–14] These parameters were obtained for different reactor configurations, of different sizes, operational under different gas types and pressures, at different driving frequencies. To propose an ICP scaling law based on these measurements is difficult because its characteristics are device specific. Since the discharge geometry strongly affects the plasma properties, it remains unclear whether a meaningful comparison can be made between data obtained in different plasma systems. Moreover, an elaborate measurement is always helpful mainly for a qualitative understanding. To enhance the transfer of knowledge and insight gained in rf discharges, a standard source (by dimension) was proposed for capacitively coupled as well as for inductively coupled rf plasmas.[9] The inductive gaseous electronics conference (GEC)-rf reference cell provides an experimental platform for comparing plasma measurements carried out in a common reactor geometry by different experimental groups.

A pure *H* mode operation is essential for the comparison between the experimental observations and the theoretical explanations, where inclusion of capacitive phenomena in a theoretical model is mathematically involved.[8,15] Often a pure *H* mode operation is also preferred under plasma pro-

[a]Author to whom correspondence should be addressed. Electronic mail: sh.v.singh@gmail.com.

cessing conditions considering low ion induced damage at the substrate level. The electrostatic coupling can be suppressed by using Faraday shields, which is an important issue of this work.[7,13,14]

The electrical characterization of the antenna parameters (namely, I_c and V_c) is often implemented into electrotechnical models, such as transformer model.[2,8,15] In this model, the power coupling in a pure H mode is described on the basis of transformer activity between the antenna (primary) coil and the assumed one-turn plasma (secondary) coil. The antenna current along with the plasma parameters, such as electron density and temperature, have been used to study the electron kinetics of ICP, and particularly of the H mode. However, the voltage drop across the antenna coil provides essential information to study the electron kinetics under an E mode operation.[16] There is considerable amount of work available describing electrical characterization of ICPs (e.g., Refs. 7–14), although a detailed work demonstrating the mode transition and hysteresis for an ICP GEC reference cell is still lacking. In an issue dedicated to the GEC-rf reference cell, an article by Miller *et al.*[9] covers constructional details of the reactor cell and electrical characterization of the inductive mode particularly, at 1.33 Pa of an argon discharge. Extensive plasma and electrical characterization for a GEC cell under different gas types is discussed in Refs. 10 and 11, but also only limited to the H mode. The electrical characterization is available on several non-GEC cells as well, but also mostly limited to H mode (e.g., Refs. 8 and 11–15). In this respect, it is essential to electrically characterize both the modes of an ICP GEC-rf reference cell.

To date, an elaborate theoretical simulation explaining the E mode operation is missing, although the capacitive branch has been included in transformer models occasionally (e.g., Refs. 2 and 15). A characterization of the antenna parameters for the E mode was initially presented by El-Fayoumi and Jones[8] for a relatively big reactor where power was coupled through a 17-turn antenna coil at a frequency of 0.56 MHz. This discharge was operated without a matching network and an attempt was made to explain the hysteresis and the mode transition by means of an electromagnetic (EM) theory and circuit analysis. Later, the power transfer efficiency and the mode transition behavior were studied for an almost similar setup but then under matched conditions.[17] In addition, a work from the same group covers electrical characterization presented in terms of changes in the plasma load resistance and reactance.[18] A clear and abrupt mode transition in terms of electron density and effective temperature was also presented in these works.

In rf discharges the external power to the plasma is coupled via electrons.[19,20] Therefore, any change in the antenna parameter will be reflected in the electron energy distribution function (EEDF). The EEDF evolution with power and pressure in a H mode is well understood and elaborately covered in the literature (e.g., Refs. 21–23). In connection to the H to E mode transition, the EEDFs in the H mode revealed that the distribution functions are bi-Maxwellian close to the transition region. This bi-Maxwellian distribution is due to the parasitic electrostatic coupling in the H to E transition region. In contrast to the H mode, investigations in the E mode are still very limited. Until recently, only a few major works have been devoted to EEDF measurements in this mode.[6,24–26] It has been reported (cf. Ref. 24) that the EEDF evolves from a bi-Maxwellian (at low pressures) to a Maxwellian (at moderate pressure) and finally to a Druyvesteyn distribution (at high pressures). This EEDF evolution has been explained on the basis of similar observations reported by Godyak and Piejek[27] for a capacitively coupled plasma (CCP). The EEDFs presented in Ref. 25 for pressures of 0.67 and 6.7 Pa are reported to be Maxwellian and Druyvesteyn-like, respectively. Moreover, we have shown that the EEDFs are bi-Maxwellian immediately before E to H and H to E mode transitions.[26] In addition, we have also shown that the E mode is characterized by two distinct regions,[6] where under low powers (presumably in the pure E mode) the EEDF evolution is identical to the one reported in Ref. 24. A complete EEDF evolution will also be discussed here in the context of electrical characterization results.

In this study, we present results on the internal plasma parameters and the external electrical operational parameters, in particular, with regard to the mode transition and hysteresis. A wide range of discharge conditions by varying applied power (up to 150 W), gas pressure (0.7–7.5 Pa), and electrostatic coupling strength are measured for an ICP GEC-rf reference cell. Argon gas has been used in the present report. The external electrical parameters such as antenna current and antenna voltage amplitudes are measured after the matching network, and their behavior is discussed for both the modes. Relatively smooth transitions are observed in the external parameters measured close to the H to E mode transition region. However, the reverse transition from E to H mode was found to be abrupt. An effect on the power coupling efficiency by varying the electrostatic coupling strength is studied via implementing two distinct grounded Faraday shields, in addition to the nonshielded condition. Plasma parameters such as electron density, electron temperature, plasma potential, floating potential, and their evolution with power are also shown and discussed. Additionally, a brief summary of EEDF evolution with power and pressure is presented with regard to mode transition and hysteresis. The EEDF evolution also indicates a gradual and relatively smooth transition of the modes. By combining these external and internal parameters, a prejump behavior in the transition region is demonstrated.

II. EXPERIMENTAL

The GEC reference cell utilized here has been described in detail elsewhere.[7,9] Briefly, the discharge cell is a cylindrical stainless-steel chamber with an inner diameter of 251 mm and a height of 222 mm (see Fig. 1). The rf (at a frequency of 13.56 MHz) power is coupled through a five turn spiral planar coil which consists of a water cooled copper tubing with outer diameter of 3 mm and 0.75 mm thick walls. The used antenna is wound by hand and has an outside diameter of ~100 mm and the consecutive turns are approximately equally spaced. The antenna is placed outside of the discharge vessel above a coupling quartz window (120 mm diameter and thickness of 9.5 mm) and is positioned 40 mm

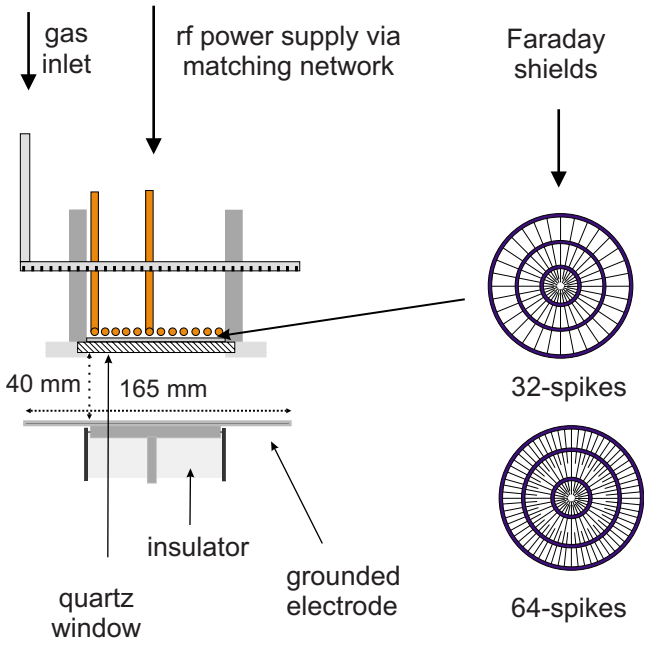

FIG. 1. (Color online) Schematic of the ICP source and the used Faraday shields.

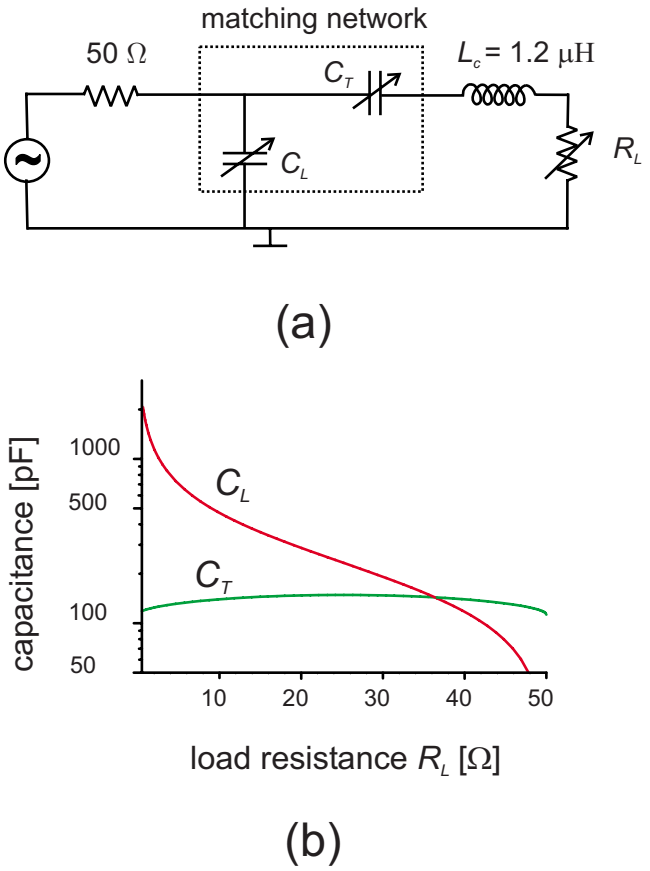

FIG. 2. (Color online) (a) Schematic diagram of the matching network. (b) Estimation for the values of matching capacitors (C_L and C_T) for an assumed purely resistive load (R_L) in place of the plasma.

above the grounded electrode. The grounded stainless-steel lower electrode is an extended electrode plate of 165 mm diameter and a thickness of 5 mm, which is placed above the original grounded electrode of 100 mm diameter.

The inductance value, $L_c = 1.22\ \mu\text{H} \pm 10\%$, of the antenna coil has been measured at the resonance frequency of a tank circuit by connecting an extra capacitor parallel to the coil. These measurements were carried out using a network analyzer and were performed with different valued capacitors. The output impedance (50 Ω) of the rf source was matched to the impedance of antenna-plasma load for maximum power transfer. A modified commercial impedance matching network was kept adjacent to the coil avoiding any extra stray inductance or resistance [see Fig. 2(a)]. The matching network consists only of high voltage vacuum capacitors. The connections inside the matching network were made using copper tubes or strips to minimize resistive losses and were convection cooled.

A substantial effort to find the right matching condition is often reported and it is a matter of separate treatment. Here, a rough calculation is made by placing a purely resistive load (R_L) on the place of plasma as presented in the circuit diagram [see Fig. 2(a)]. In the calculation, the matching capacitor C_T needs very little adjustment, whereas the other capacitor C_L changes drastically with any alteration in the dummy resistive load which was placed to simulate the plasma impedance, as shown in Fig. 2(b). Very similar changes in C_L and C_T have been observed in the experiments as well during the plasma operations.

To suppress the electrostatic coupling during plasma operation, two different grounded Faraday shields were used and were placed between the antenna coil and the quartz coupling window. The Faraday shields used were made up of stainless steel with a thickness of 3 mm and consist of 32- and 64-star shaped radial spikes, respectively (cf. Fig. 1). The spikes are mechanically stabilized with the help of two ceramic rings.

Figure 3 depicts the measurement scheme used for the experiments. Rf current flowing in the external circuit has been monitored using homebuilt Rogowski coils at two distinct places, namely G and R.[7,28] Measurement point G lies before the matching network to characterize the rf current delivered by the power generator. Point R lies between the matching network and the coil to characterize the current flowing through the antenna coil. Simultaneously, rf voltages were also monitored at the same positions using capacitor voltage dividers calibrated by a commercial voltage probe.[7,29] The current and voltage probes were calibrated at 13.56 MHz using the same generator which has been used as

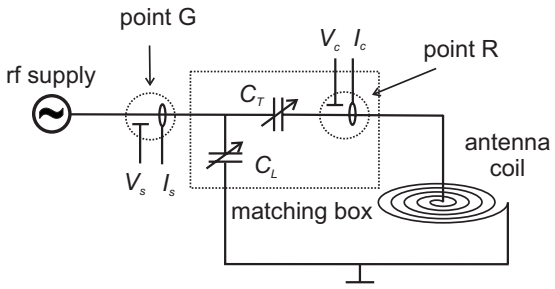

FIG. 3. Schematic of the measurement scheme for the electrical characterization.

the rf power source during the experiments. This generator can deliver a maximum power of 1200 W (at 13.56 MHz), although for this work the power was limited only up to 150 W. Since the current-voltage measurements at point *G* corroborate the power supplied by the generator, only the results of measurements at point *R* are presented.

The resistive losses in the antenna and in the associated hardware are determined by equating the measured input power to the $I_c^2 R_c$ at the matched-impedance operation under high-vacuum conditions without any discharge.[9] R_c is the effective resistance responsible for the power loss, since no power is absorbed by the plasma in the absence of any discharge. As mentioned earlier, due to the used high-vacuum capacitors and appropriate connections in the matching network, the resistive losses were minimal in the matching unit. Hence no such losses are included in these calculations. The value of R_c is quite dependent on the used Faraday shield. It has been reported elsewhere that the power coupling to the plasma is sensitive to the spacing between the antenna and the quartz window.[9] In the present work, this spacing is kept constant for plasma operations with and without Faraday shield. In order to maintain the gap in the absence of a Faraday shield, a Teflon spacing ring of similar dimensions as the shield was used. The value of $R_c = 0.59\ \Omega$ was measured for the setup without any Faraday shield, whereas increased values of $R_c = 0.74\ \Omega$ and $R_c = 0.78\ \Omega$ were measured for the setup with installed Faraday shield of 32-star-shaped spikes and 64-star-shaped spikes, respectively. The value of R_c under unshielded condition is close to the one reported in Ref. 9.

The phase angles between antenna current and voltage at the measurement point *R* were quite close to 90°, and consequently, they could not be measured with sufficient accuracy. The phase difference between current and voltage measurement at point *G* was around zero as expected.

A commercial Langmuir probe is used to measure the plasma parameters and its constructional details are described elsewhere.[7] Briefly, the probe tip of the system consists of a thin metal wire of a diameter ranging from 50 to 100 μm. Measurements in the *H* mode and in the *H* to *E* mode transition region were performed using a 50 μm diameter tip. Due to almost two orders of magnitude lower electron density to be probed, the tips were replaced by 100 μm thick wires in the *E* mode and in the *E* to *H* mode transition region. The length of the tip was fixed at around 9 mm under all the conditions. To avoid rf distortions in the probe current-voltage scans, tuned rf filters in combination with software low pass filters were used to maximize the rf impedance of the probe tip to the ground.[30]

The probe current is calculated according to the orbital motion limited theory under the assumption that the movement in the space charge layer is collisionless. Druyvesteyn's method is used for the determination of the EEDF.[31] The electron energy distributions measured in this study are presented in terms of the electron energy probability function (EEPF) (in units of $\mathrm{cm}^{-3}\ \mathrm{eV}^{-3/2}$) rather than the EEDF.[7] The EEPF is obtained from the second derivative of the Langmuir probe characteristic in the electron retardation regime ($V_s \leq V_p$, where V_s is the probe potential and V_p is the plasma potential) according to

$$f(\varepsilon) = \frac{2m_e}{e^2 A_p}\sqrt{\left[\frac{2e}{m_e}\right]}\frac{d^2 I}{dU^2}, \tag{1}$$

where I, A_p, e, and m_e are the probe current, probe tip area, electron charge, and electron mass, respectively. The $U = V_p - V_s$ is the probe potential with respect to the plasma potential. The zero crossing of the second derivative of the probe current is assumed to be the dc value of the plasma potential, whereas the zero crossing of the current in the characteristic curve is the floating potential of the probe. EEDF, plasma density, and mean kinetic energy are given by

$$F(\varepsilon) = \sqrt{\varepsilon} f(\varepsilon), \tag{2}$$

$$n_e = \int_0^{\varepsilon_{\max}} F(\varepsilon)\varepsilon, \tag{3}$$

$$\langle \varepsilon \rangle = n_e^{-1} \int_0^{\varepsilon_{\max}} \varepsilon F(\varepsilon) d\varepsilon. \tag{4}$$

The kinetic energy ε in these equations is equal to U.

III. RESULTS AND DISCUSSIONS

A. Electrostatic shielding and plasma parameters

The influence of three distinct electrostatic coupling arrangements on the plasma parameters is demonstrated in this section. The results presented in Fig. 4(a) are aimed to demonstrate the effectiveness of the utilized Faraday shields. Although the electrostatic coupling dominates at low powers, specifically in the *E* mode operation, but its presence in the *H* mode (especially in the vicinity of *H* to *E* mode transition) is quite critical for certain industrial applications.[3] Since the *E* mode is by nature similar to a CCP, it is characterized by a relatively high plasma and floating potential compared to the *H* mode. Therefore, a comparison of plasma potential between unshielded and shielded (by placing Faraday shield) ICPs could very well indicate the presence of stray capacitive coupling in *H* mode.

In Fig. 4(a), the measured plasma potentials in the *H* mode but also close to *H* to *E* mode transition region (being in *H* mode) is presented for 1.3 Pa. The increased plasma potential close to the transition region clearly displays the dominance of electrostatic coupling in the region. Moreover, the significance of a Faraday shield is revealed by the decreased plasma potential values after its introduction. The decrease in the plasma potential is obvious for the 32-spiked Faraday shield compared to the nonshielded setup, while a further improvement can be seen for the setup with 64 spikes. The decrease in plasma potential immediately before the *H* to *E* mode transition point (at 45 W) between the nonshielded and shielded ICPs is noticeable. It reveals a clear decrease from ~27.5 to ~23 V between the nonshielded to the 64-spiked Faraday shielded setup. However, the plasma potential for all three setups remained relatively low at higher powers in pure *H* mode and the differences are

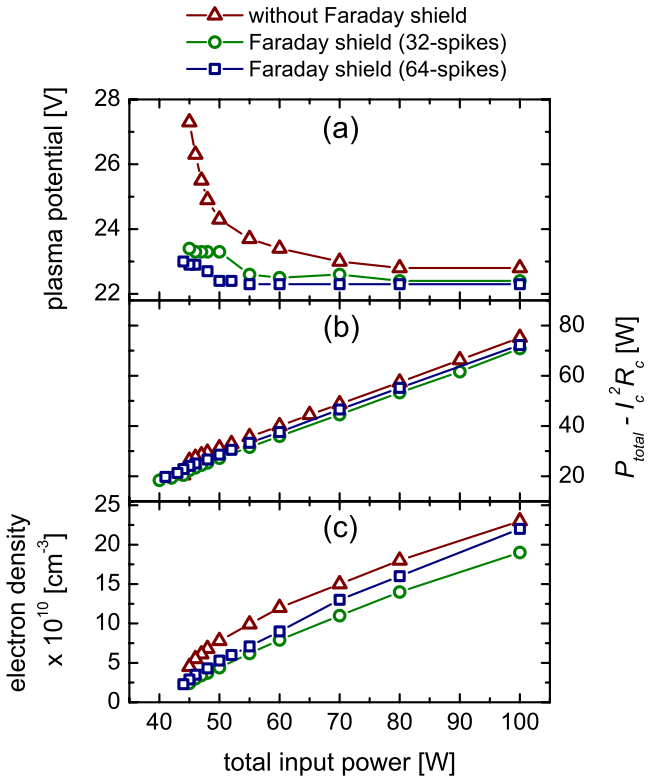

FIG. 4. (Color online) Plasma parameters in the *H* mode (a) plasma potential (partially taken from Ref. 6, the symbol size also represents the error bar in the data), (b) real power coupling, and (c) electron density.

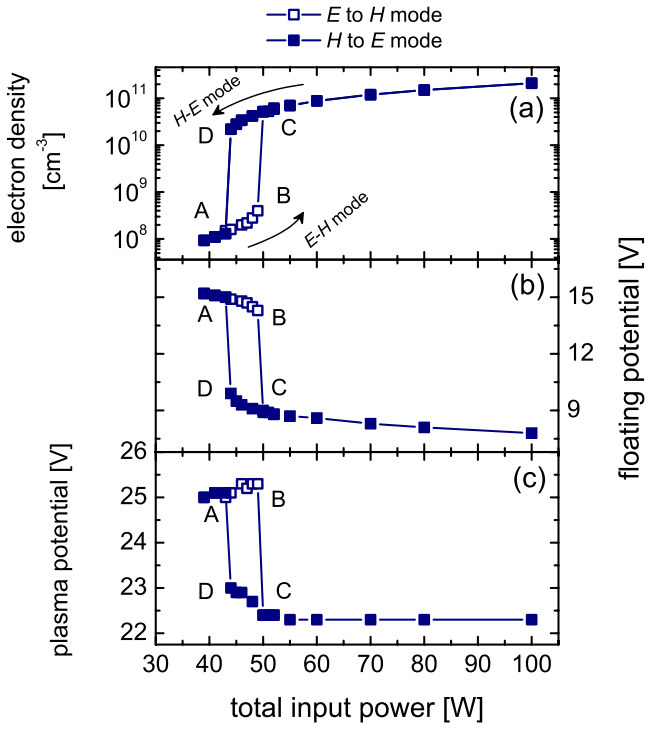

FIG. 5. (Color online) Plasma parameters demonstrating the mode transition and hysteresis, (a) electron density, (b) floating potential, and (c) plasma potential.

almost within the error bar. An almost identical and low plasma potential indicates that the parasitic electrostatic coupling is shielded due to the increased electron density at higher powers [cf. Fig. 4(c)].[2] In this respect a similar trend has been observed for other pressures as well.

Power losses in the external components and the dependence of electron density on the efficiency of power coupling to the plasma are presented in Figs. 4(b) and 4(c). It is difficult to comment on the real power coupled to the discharge by the antenna. Since the power supplied by the generator is not the effective power coupled into the plasma, a distinction has been made between these two powers. The power supplied by the rf generator is referred to as the total input power (P_{total}). While, the power measured after the matching is referred to as the real power coupled to the plasma, which is equal to the external losses subtracted from the total power $P_{\text{total}} - \frac{1}{2}(I_c^2 R_c)$. Taking the external losses $\left[\frac{1}{2}(I_c^2 R_c)\right]$ into account, the effect of Faraday shield on the power coupling to the plasma is presented in Fig. 4(b). Note that all the measurements have been performed under matched conditions with 0 W reflection power. The resistive losses occur due in part to the Eddy currents induced in the stainless-steel cylinder that surrounds the antenna coil. These losses are almost 50% in the dominant electrostatic coupling region compared to around 25% loss in the pure *H* mode.

The measured power coupling does not significantly differ among the three different setups. Because of the low R_c, the external losses were least for the setup without any Faraday shield. However, external losses are smaller for the setup with the Faraday shield of 64 spikes in comparison to the one of 32 spikes, albeit that the R_c is highest for the setup with Faraday shield of 64 spikes. This behavior can be explained by a remarkable decrease in the antenna current when using a better shielding, which will be discussed later. In addition, it is found that the electron density in the *H* mode is directly proportional to the applied power. Moreover, the results reveal that the power coupling to the plasma in the *H* mode is better and purer inductive under good Faraday shielding.

The mode transition and hysteresis are often illustrated in terms of the electron density with respect to the applied rf power to the antenna coil (e.g., Refs. 2, 4, 17, and 18). Note that the measurements presented in Fig. 5 are performed with the 64-spiked Faraday shield installed and hence under good electrostatic field shielding. Under these conditions the discharge was initiated using an external ignition source working on the principles of a sparking plug. At low powers (corresponding to $n_e \approx 10^8 - 10^9$ cm^{-3}) the discharge operates in the capacitive *E* mode, see Fig. 5(a). Increase in the rf power shifts the discharge from the capacitive mode through a capacitive-inductive transition (mixed *E-H*) regime which finally jumps into the inductive mode, at point *B* (~49 W). In the inductive *H* mode, the electron density ($\approx 10^{11}$ cm^{-3}) jumps by almost two orders of magnitude which eventually brings the system to point *C*. The discharge stays in the *H* mode when further increasing the power. The reverse transition occurs at point *D* (~41 W) at a relatively low power instead of point *C* (the *E* to *H* transition point) after passing through the inductive-capacitive transition regime, causing hysteresis. A strong simultaneous mixing of capacitive and inductive heating has been reported for the power region adjacent to both the transition points, e.g., Refs. 2, 4, 5, and

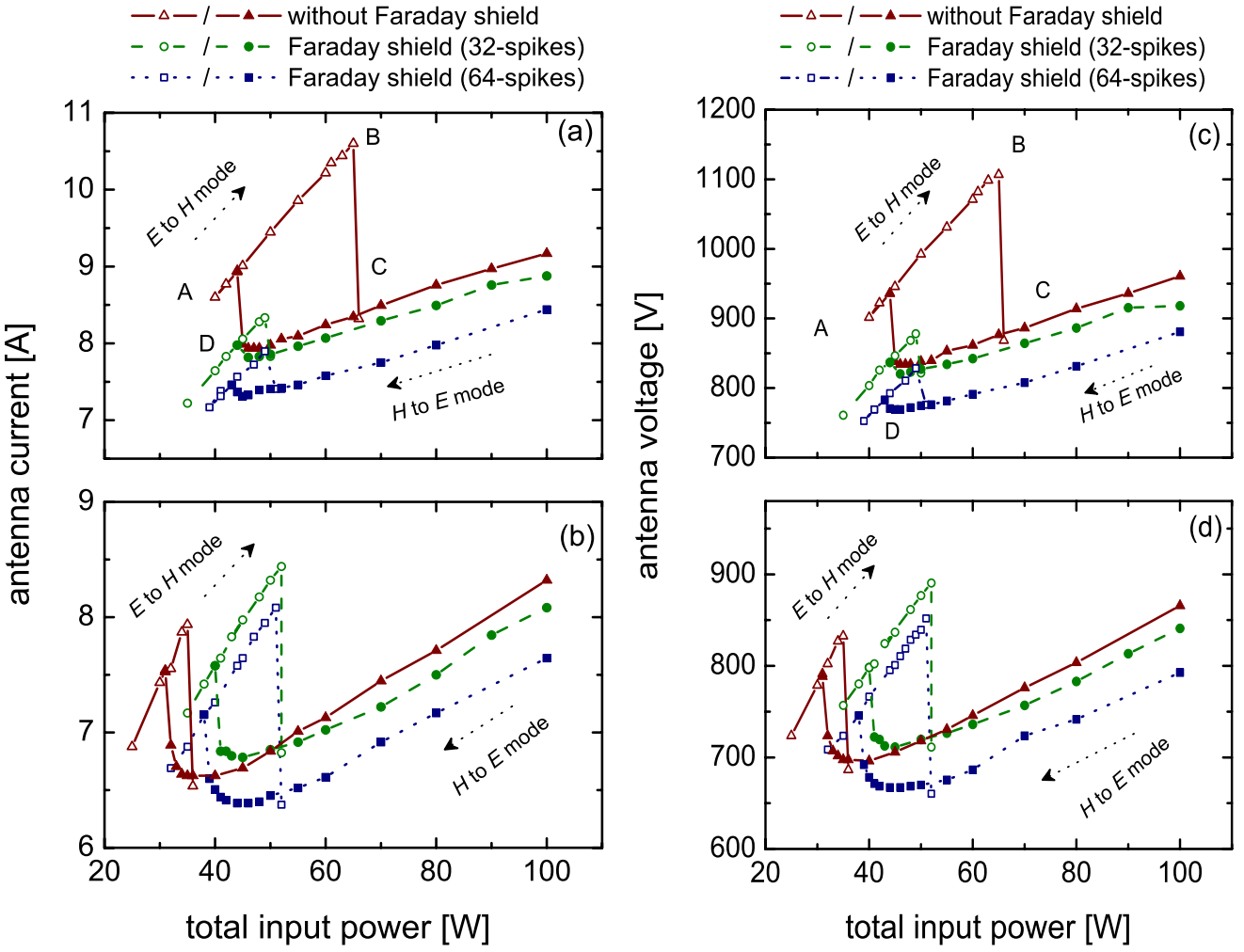

FIG. 6. (Color online) Measured antenna parameters for the setup with the different Faraday shields. The antenna current amplitudes at (a) 1.3 Pa and (b) 5 Pa. The antenna voltage amplitudes at (c) 1.3 Pa and (d) 5 Pa.

22. Although this hybrid region cannot discretely be separated, however, considering its dominance in the hysteresis loop *ABCD* (as shown in Fig. 5), it will be referred as a "mixed" or "hybrid" mode regime in this study. To keep the explanations simple throughout the article a similar notation for the transition points *A*, *B*, *C*, and *D* will be followed. Similar to the mode transition and hysteresis, the presence of the mixed mode has also been reported in every plasma parameter and is observed as a gradual change in the regions *AB* and *CD*. The mode transition and hysteresis are also observed for the plasma and floating potential measurements, as shown in Figs. 5(b) and 5(c). The floating potential remains around 15 V in the *E* mode and around 10 V in the *H* mode, whereas the plasma potentials in *E* mode are measured around 25 V and around 22 V in *H* mode.

B. Mode transition and hysteresis via antenna parameters

The phenomena of mode transition and hysteresis obtained for the plasma parameters are also observed in the antenna current and voltage measurements. These time varying antenna parameters are presented in terms of their amplitude values in this study. The measured hysteresis loop for the antenna current and voltage amplitude is shown in Fig. 6 [via points *ABCD*, as defined in Fig. 5(a)], respectively. The measurements are presented for two gas pressures, namely 1.3 and 5 Pa. For a fixed pressure, the antenna current decreases with the decrease in the total input power when operating in *H* mode and jumps to a relatively high current together with the jump into the *E* mode [see Figs. 6(a) and 6(b)]. For the same P_{total}, the current in the *E* mode is higher than the current in the *H* mode and it further increases with an increase in P_{total}; meaning that the *E* to *H* mode transition occurs at a significantly high current. A similar behavior has been observed for the antenna voltage as well, see Figs. 6(c) and 6(d). Without Faraday shield the *E* to *H* mode transition occurs at $I_c \sim 10.6$ A and $V_c \sim 1106$ V, whereas the *H* to *E* mode transition happens at $I_c \sim 8$ A and $V_c \sim 838$ V for 1.3 Pa. A similar trend has been measured for all three different electrostatic coupling arrangements. For the setups with Faraday shield, the width of the hysteresis loop increases with increasing pressure within the range of gas pressure covered in this study. The widths are almost about 6 W at 1.3 Pa and about 29 W at 7.5 Pa under the operation with the best Faraday shield (64-spiked). Similar observations on the plasma parameters with regard to pressure have been already published.[25] The hysteresis width is least for the Faraday

shield of 64 spikes throughout the pressure range. However, no such clear trend could be obtained for the measurements without shielding in this pressure range.

Figure 6 also extends the understanding on the effectiveness of a Faraday shield. Due to the implementation of a Faraday shield, the antenna current and voltage amplitudes show a clear decrease over all the input power range. The amplitudes are least for the setup with 64-spiked Faraday shield installed. Furthermore, the antenna parameters for both the transition points E to H and H to E (points C and D) were also lowest for the discharges with this Faraday shield. For example, at 1.3 Pa, the antenna parameters for the point C are $I_c \sim 7.9$ A and $V_c \sim 828$ V, whereas for the point D the antenna parameters are $I_c \sim 7.3$ A and $V_c \sim 770$ V. These were followed by the setup with 32-spiked Faraday shield, where E to H transition occurs at $I_c \sim 8.3$ A and $V_c \sim 878$ V and H to E transition occurs at $I_c \sim 7.8$ A and $V_c \sim 822$ V for 1.3 Pa. The differences between two extreme electrostatic coupling conditions in terms of antenna parameters are noticeable. For example, at 1.3 Pa the differences for E to H transition are $\Delta I_c \sim 2.5$ A and $\Delta V_c \sim 278$ V, whereas the differences for H to E transition are $\Delta I_c \sim 0.7$ A and $\Delta V_c \sim 68$ V. Lowering of antenna current and voltage amplitudes by the implementation of different shields clearly indicates the effectiveness of the Faraday shielding. Moreover, a relatively small difference under all the three experimental arrangements during the H to E transition supports its minimal influence on the H mode operation. Although, the R_c value increases significantly with the introduction of Faraday shields (cf. experimental) due to a significant decrease in the antenna current, the voltage drop across the coil also decreases. The decrease in current due to the introduction of Faraday shields could explain why only a nominal difference in power loss among the three distinct setups is observed (cf. Fig. 4).

Because the rf generator impedance was matched to the plasma impedance, the measured antenna current and voltage amplitudes were quite high. The phase difference between them is very close to 90° and hence could not be measured with sufficient accuracy. In Fig. 7, the calculated phase angle is being presented where the calculations are made using[9] $P_{\text{total}} - \frac{1}{2} I_c^2 R_c = \frac{1}{2} I_c V_c \cos(\phi)$. Note that no resistive losses in the matching unit are included in these calculations as well. In general, the phase decreases with increasing power and the phases were least for the best electrostatically shielded setup.

Due to the scientific and technological demands, the ICP operation with minimal electrostatic coupling is more interesting. Since the electrostatic shielding was the best for the setup with 64-spiked Faraday shield, detailed results are presented for this reactor arrangement. The antenna current and voltage with respect to the gas pressure for the best electrostatically shielded setup are depicted in Fig. 8. The antenna current values measured for the same input power in the H mode decrease significantly with the increase in gas pressure and, therefore, the H to E mode transition appears at lower current values for higher pressures [see Fig. 8(a)]. A similar trend of a decrease in the antenna current values for pressures with a marginal difference has been observed for the E mode as well. The hysteresis width increases with increasing gas pressure because the H to E transition occurs at lower current values, whereas the E to H transition results at larger current values for higher pressures. The trend of the antenna

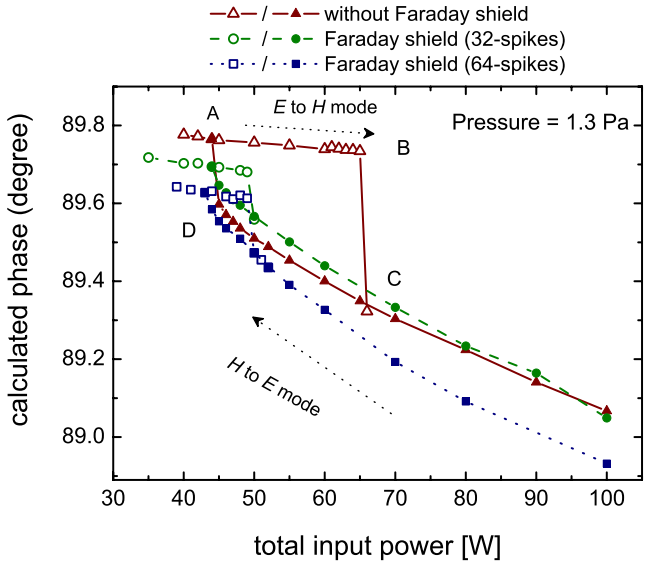

FIG. 7. (Color online) Calculated phase between the antenna current and antenna voltage.

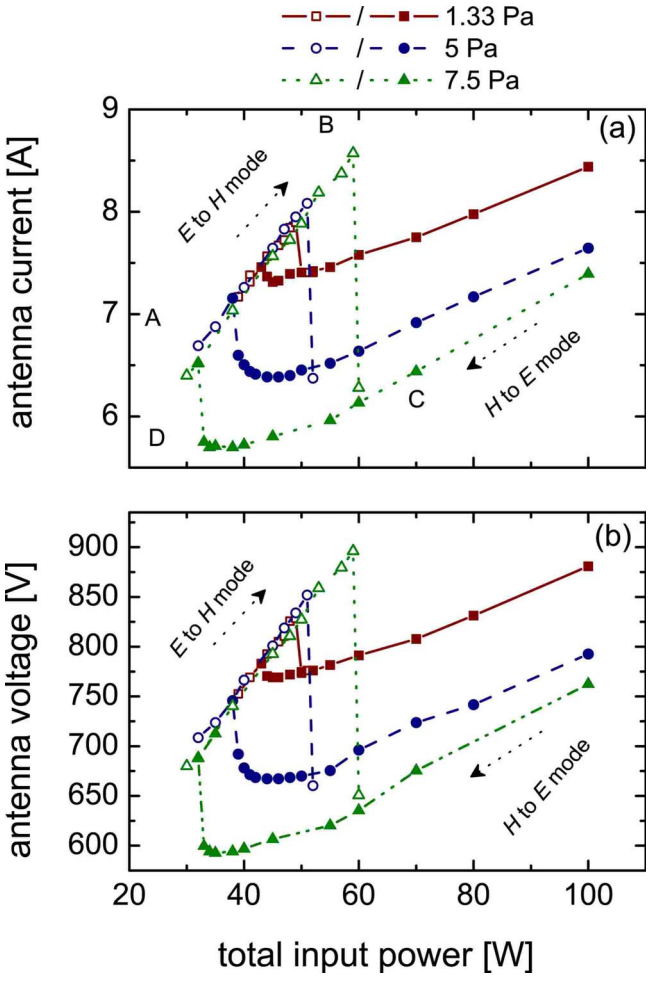

FIG. 8. (Color online) Measured (a) antenna current amplitudes and (b) antenna voltage amplitudes at different pressures.

voltage with respect to the total input power is qualitatively similar to that of the antenna current [see Fig. 8(b)]. It also reveals a similar increase in the hysteresis width with increasing gas pressure. The H to E transition occurs at lower voltage values, whereas the E to H transition results at larger voltage values for higher pressures.

The implementation of Faraday shields reduced the generated antenna current and the voltage drop across it and hence reduced the power deposited capacitively because of the electrostatic coupling. Even with an increased external resistance (R_c), the resistive external losses remained virtually constant compared to the other arrangement because of the reduced antenna current. Note that the reduced antenna current indicates an improved inductive coupling between the coil current and the plasma. The phase angle between the antenna current and voltage has been found to be very close to 90° (cf. Fig. 7).

Moreover, the most important conclusion can be made by following the antenna current and voltage close to the H to E mode transition (mixed mode) region. In this region antenna parameters start to behave reversely even under H mode operation, meaning that they increase with the decreasing power before finally jumping into relatively high (corresponding) values in the E mode. This reverse trend near the H to E transition region can be considered as a prejump region. The prejump changes are as high as $\Delta I_c \sim 0.5$ A and $\Delta V_c \sim 25$ V. No such prejump behavior near the E to H mode transition could be resolved in the measured antenna parameters. On the other hand, this gradual change (categorized as a prejump behavior) has also been observed close to both the transition points in the obtained plasma parameters, such as electron density and potentials (cf. Fig. 5).

The prejump behavior in EEDFs close to the H to E transitional mixed mode region is a well known phenomenon. Recently, we have shown a similar prejump behavior in terms of EEDF for the E to H transitional mixed mode region as well. The presence of electrostatic coupling revealed by a measured bi-Maxwellian EEDF in the hybrid region of the H mode is well established. Likewise, the trend of a reverse increase (prejump region) in antenna current in this region can be attributed to the appearance of electrostatic coupling already in the H mode operation. As a result the current starts to increase already in the H mode instead of further decreasing before it finally jumps to the high values that are characteristic for the E mode. To illustrate the prejump behavior adjacent to E to H transition region in terms of the EEDF evolution along the hysteresis cycle is presented in the next section.

C. Mode transition in terms of EEPF

The EEDF results summarized in this section are elaborately discussed in our previous work.[6,26] Here we critically consider the whole issue in context to the hysteresis loop, mainly to illustrate the prejump behavior in our electrical characterization results. These EEDF results are summarized together in Fig. 9. For a pure H mode, the EEPF evolution is mostly reported to be dependent on the gas pressure, which is depicted in insert I of Fig. 9. The EEPFs are bi-Maxwellian at low pressures and evolve into a Maxwellian distribution with increasing pressure, for the same power. However, with a further increase in pressure the EEPF develops into a Druyvesteyn distribution. This EEPF evolution can be explained on the basis of collisionless heating through the skin layer, the Ramsauer minimum in argon, and (linear to nonlinear) electron diffusion processes as reported in several works, e.g., Refs. 21, 32, and 33. Moreover, for the range covered in this study the shape of the normalized EEPF in a pure H mode is independent of the increasing power explaining no alteration in the power coupling mechanism to the electrons.

The EEPF evolution with decreasing power and particularly in the vicinity of the H to E mode transitional hybrid region is noticeable, revealing the prejump behavior. The EEPFs have an evident two-temperature structure as shown by the measurements for the typical discharge setup, as summarized in inserts I and II of Fig. 9. The measured bi-Maxwellian distribution (Fig. 9 insert II) can be interpreted in an analogy to two-temperature distribution functions of a parallel plate capacitively coupled rf argon discharge.[20,22] This distribution originates from the two electron heating mechanisms involved in a CCP, i.e., the stochastic heating adjacent to the sheath and the Ohmic heating in the plasma bulk. Close to the H to E transition region because of decreased n_e sheaths are appreciable, consequently, the electrostatic coupling due to the high voltage drop across the sheath starts to appear. This coupling translates in antenna parameters as a prejump behavior. Hence the presence of the overpopulated low energy electron group is being referred to the stochastic heating in the developed oscillating sheath and to the nonlocal electron kinetics in the low pressure discharge conditions. The transition from a concave distribution function at lower powers to a Maxwellian or Druyvesteyn distribution (depending on the pressure) at higher powers is caused by the shielding of electrostatic field and high electron-electron collision frequency, $\nu_{ee}(\propto n_e/T_e^{3/2})$, which is a result of an increase in n_e with increasing power.

By summarizing the available reports in the literature on the EEDFs in an E mode, results reveal that the EEDF evolves from a bi-Maxwellian (at low pressures) to a Maxwellian (at moderate pressure) and finally to a Druyvesteyn distribution (at high pressures).[6,24,25] Due to the low electron density and small (power) range of operation, often these measurements are performed close to the E to H transitional hybrid region. Note that the E-H mode mixing is high in the transition region and the modification of EEDF is most likely in this power region. Furthermore, the width of the hysteresis loop is found to be pressure dependent (much smaller in the case of low pressure). Therefore, performing measurements at one fixed power in the E mode will not fairly reflect the similar power coupling conditions under different pressures. This issue is often not contemplated.

To avoid the ambiguity about the power coupling because of the pressure, two distinct power regions (points) were selected in our recent work.[6] The first point is at the power immediately after the H to E jump in the E mode (point A, Fig. 9) and the second point is immediately before the E to H mode jump (point B, Fig. 9). We believe that the

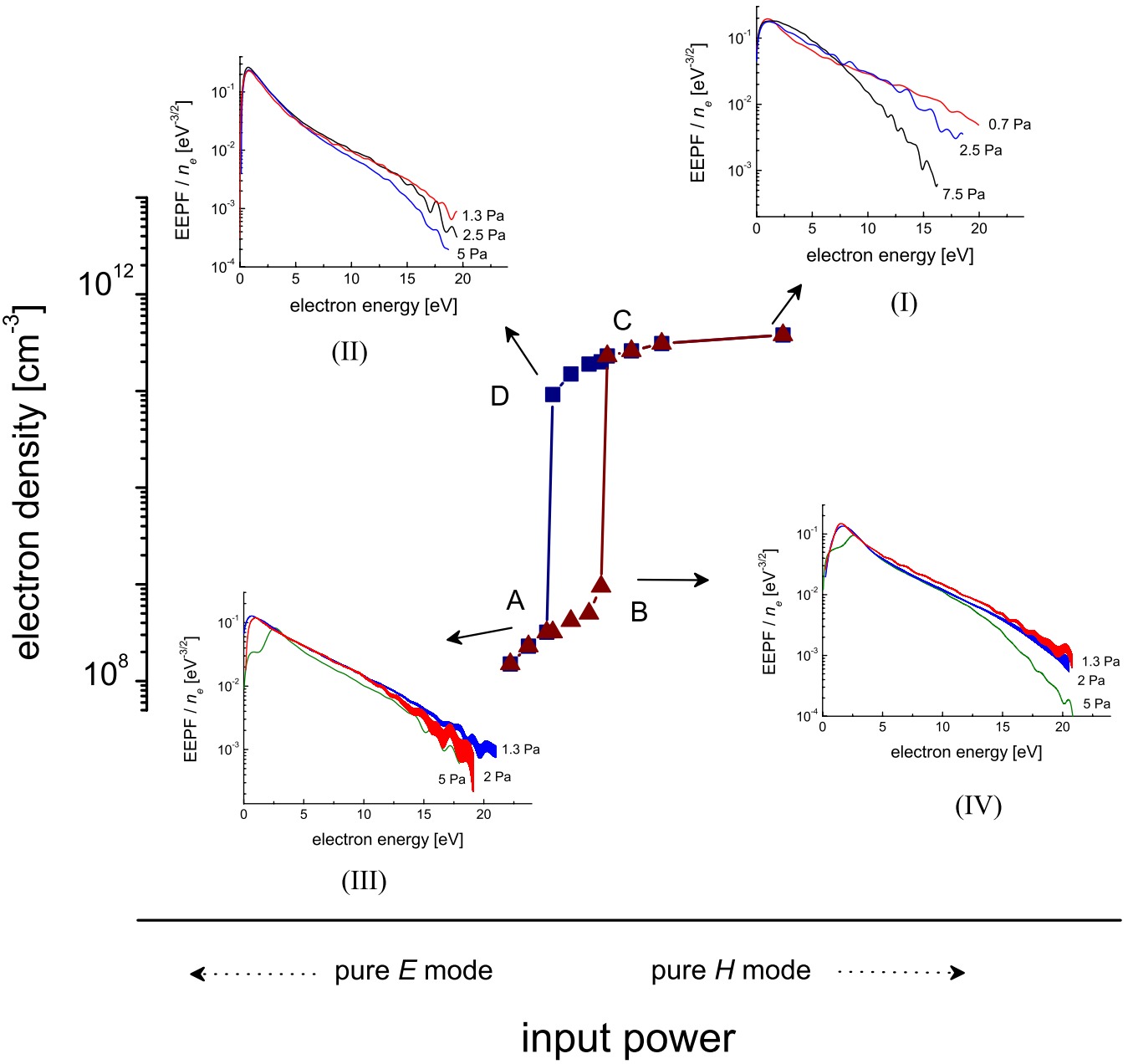

FIG. 9. (Color online) EEPF evolution along the hysteresis loop (partially taken from Refs. 6 and 23).

first measurement point represents a pure *E* mode, whereas the second one represents the mixed mode region of an *E* mode operation.

As shown in insert III of Fig. 9, the EEPFs evolve from a Maxwellian to a Druyvesteyn-like distribution at low powers of the so-called pure *E* mode operation. As depicted by Chung and Chang,[24] this heating mode transition from collisionless (stochastic) heating at low pressure to collisional heating at high pressure is in line with the observations of Godyak and Piejak[27] for a CCP. Note that the differences in operational rf frequency and the different setup used in Ref. 24 could be a possible reason for the minute variations from our results.

The measured EEPF within the mixed mode (immediately before the *E* to *H* transition) region at low pressures is distinctively concave in nature (Fig. 9, insert IV) compared to a Maxwellian at very low powers. These results reveal alterations that are presumably identical to the prejump behavior observed for the reverse transition region. The EEPFs in this power regime are bi-Maxwellian even at pressures as high as 3 Pa, in contrary to the collision dominant with almost Druyvesteyn-like distribution in a pure *H* or *E* mode. (Measurements at high pressures, e.g., at 5 Pa were difficult with regard to the resolution of low energy electrons in the EEPF, which is a well known problem associated with probes under such conditions.) These result with regard to EEPF evolution has not been very well understood, however, they indicate to the presence of a prejump mechanism in this region. Recently, we attributed the observed bi-Maxwellian EEPF to the increase of an extra heating process identical in nature to the stochastic heating process.[6]

An obvious concave EEPF even at relatively high pressures clearly indicates alterations in the heating mechanism in the mode transition region. Since E mode is already working under the influence of an enhanced capacitive sheath, as predicted in Ref. 24, the increased contribution of low energy electrons in insert IV of Fig. 9 needs further investigation. The possibility of $\alpha-\gamma$ transition due to a comparatively high voltage drop (near the transition region) across the antenna has been studied, and such transitions have been discounted due to low current densities.[2,7] Furthermore, multistep ionization might also induce similar effect but is essentially negligible at the pressures studied.[2,26,34] Hence these results obtained close to the mode transition region could be attributed to the strong alterations in power coupling inducing effects similar in nature to stochastic heating.[6]

On the basis of data available in the literature on direct EM field measurements, we recently proposed a simple Poynting vector representation.[6] Using this heuristic approach, the possibility of strong alterations close to the mode transition region can be easily demonstrated. It is known that the Poynting vector $(\vec{E}\times\vec{B})$ gives the direction and the average energy transfer by an EM field per unit time, per unit area in an inductive discharge.[8,35] The typical planar induction coil excites $\{B_r,B_\theta,B_z\}$ and $\{E_r,E_\theta,E_z\}$ (radial, azimuthal, and axial) magnetic and electric field components, respectively.[8,16,19] These fields are basically complex quantities, and inclusion of the phase relation among them will be quite complicated. Therefore to avoid the complications of heavy mathematics, we presented the Poynting vector in terms of real field amplitudes only. Under these simplifications, the Poynting vector including all the planar coil field components can be written as

$$\mu_0\vec{S}_T=(\vec{E}\times\vec{B})_T=\vec{e}_r(E_\theta B_z-E_z B_\theta)-\vec{e}_\theta(E_r B_z-E_z B_r)+\vec{e}_z(E_r B_\theta-B_r E_\theta). \quad (5)$$

Furthermore, we have shown that the Poynting vector for the H mode is represented by $\mu_0\vec{S}_H=(\vec{E}\times\vec{B})_H=\vec{e}_r(E_\theta B_z)-\vec{e}_z(B_r E_\theta)$, whereas for the E mode it is given by $\mu_0\vec{S}_E=(\vec{E}\times\vec{B})_E=-\vec{e}_r(E_z B_\theta)+\vec{e}_z(E_r B_\theta)$.[6] In addition, we also proposed that in the hybrid power region all possible field components generated by a planar antenna coil are present in a considerable strength and the Poynting vector reads the same as in Eq. (5). A contrasting difference between the Poynting vectors for the pure E and H modes to the hybrid mode is the appearance of an azimuthal component $\vec{e}_r(E_r B_z-E_z B_r)$. In the presence of strong induction effects due to high electron density, the influence of this azimuthal term is negligible in H mode. However, this term might be an extra source of power coupling in the hybrid region of an E mode.[6]

The current-voltage measurement shows no (expected) decrease in the hybrid region of E mode (segment AB, cf. Figs. 6–8) to complement the prejump behavior as observed in the hybrid regime of H mode (segment CD, cf. Figs. 6–8). Moreover, the continuous increase in the antenna current and voltage amplitudes in the hybrid region of E mode might lead to a continuous increase in the azimuthal component. These results are in line with the observed increase in the reported EM field components B_r, B_z, E_r, and E_z, but its influence has always been ignored.[2,16,17,20,36] Based on the Poynting vector representation, we heuristically proposed that this extra azimuthal $\vec{e}_\theta$ component could be an extra power source which might induce such phenomenon.[6] The effect of $\vec{e}_\theta$ in the hybrid region is predicted to play similar role at several other occasions. For example, Ostrikov *et al.*[36] mentioned the plausibility of an increased source of extra heating based on their E_z and B_z measurements in the E mode "..The amplitude of the magnetic field B_Z, which is associated with TE EM mode that sustains the discharge in the H regime, increases significantly while the discharge is still in the electrostatic mode. We can thus infer that only a certain proportion of power is stored in the low-density plasma and the electrostatic field (mainly E_z) in the sheath. The rest of the power delivered by the coil is spent in increasing the EM-field energy in the chamber. As soon as the power accumulated in the EM field becomes sufficient to sustain the high-density discharge mode, a breakdown in the H mode takes place…" This predicted source of EM field energy accumulation could be due to increasing azimuthal component under discussion.

The $\vec{e}_\theta$ component will act parallel to the planar coil of the typical setup and can be compared to an externally applied field parallel to the electrodes of a CCP. The effect of such an applied parallel field component, externally or inherited (Refs. 37 and 38 and references therein), has been studied for the CCPs, and authors have observed an enhanced extra electron heating component. Interestingly, Chabert *et al.*[37] reported the presence of inductive heating and even a mode transition for parallel plate capacitively coupled discharges operating at very high frequencies identical to the E to H transition of inductively coupled discharges. Note that these results are obtained under the conditions where EM effects are significant and a direct comparison is irrelevant. Moreover, they report that under these conditions the electric field splits into two components: (i) a component perpendicular to the electrodes and (ii) a component parallel to the electrodes. There, the E mode is referred to a traditional capacitive discharge sustained by the former electric field, while the H mode is referred to the plasma sustained by the later electric field component. This transition is reported to occur at high applied voltages where the parallel heating component starts to dominate, and the transition is attributed to the extra heating component as a result of the parallel electric field component. Similarly, the measured extra low energy electrons (shown in Fig. 9, insert IV) even at relatively high pressure in the E mode can be an attribution of the extra induced $\vec{e}_\theta$ component. It can be interpreted as a possible prejump behavior in this region. Note that all the EM field components generated by a planar coil are involved in this hybrid region. But, due to presumably weak strength of the components indicating prejump behavior, the influence of these components on the antenna current and voltage measurements could not be resolved in this region.

IV. CONCLUSIONS

A complete evolution of the antenna current and voltage amplitudes with regard to distinct modes and hysteresis of an

ICP are measured. The measurements are performed after the matching network to directly relate these results with the power coupled to the discharge. A wide range of discharge conditions by varying the applied power, the gas pressure, and the electrostatic coupling are measured for a GEC-rf reference cell. Similar to the internal plasma parameters a clear mode jump and hysteresis were observed for the antenna parameters as well. The effect on the power coupling efficiency for different strengths of the electrostatic coupling is studied by implementing two different grounded Faraday shields, in addition to the original nonshielded setup. The results indicate that the implementation of a Faraday shield did increase the stray resistance of the system. Nevertheless, the power coupling did not change as far as the *H* mode is concerned. This has been attributed to reduced antenna current and voltage under good electrostatic shielding. The width of the hysteresis loop under the electrostatic shielded discharge operation increases with increase in gas pressure. It is due to the decrease in antenna current and voltage amplitudes for the *H* to *E* transition and increase in these parameters for the *E* to *H* transition with increasing pressure.

Like the plasma parameters, a relatively smooth transition is observed in the external parameters measured close to the *H* to *E* mode transition region. Contrary to the trends of plasma parameters, however, the reverse transition from *E* to *H* mode, was found to be abrupt in the antenna current and voltage measurements. Keeping in with the goal of this paper a brief summary of electron energy distribution function, electron density, floating potential, and plasma potential evolution with power and pressure is also presented with regard to the mode transition and hysteresis. An effort has been made to relate them to the results obtained for the external parameters. The EEDFs immediately before the mode jump have been reported to be identical, namely bi-Maxwellian. We expect that these measurements can be helpful in developing theoretical models specifically for the fewer known *E* mode.

ACKNOWLEDGMENTS

The authors gratefully acknowledge Professor Dr. H. Soltwisch from Ruhr University Bochum for giving opportunity to work in his Arbeitsgruppe, and Sonderforschungsbereich 591 of the Deutsche Forchungsgemeinschaft for the financial support. The skillful technical assistance of Mr. B. Becker and Mr. T. Zierow is also greatly appreciated. We would also like to thank Dr. S. Agrawal-Singh and Dr. E. Langereis for critical reading of the manuscript. The experimental work was done at Institut für Experimentalphysik V, Ruhr-Unversität Bochum, Universitätsstr. 150, 44780 Bochum, Germany.

[1]J. Hopwood, Plasma Sources Sci. Technol. **1**, 109 (1992).
[2]M. M. Turner and M. A. Lieberman, Plasma Sources Sci. Technol. **8**, 313 (1999).
[3]M. Osiac, T. Schwartz-Selinger, D. O'Connell, B. Heil, Z. Lj. Petrovic, M. M. Turner, T. Gans, and U. Czarnetzki, Plasma Sources Sci. Technol. **16**, 355 (2007).
[4]U. Kortshagen, N. D. Gibson, and J. E. Lawler, J. Phys. D **29**, 1224 (1996).
[5]K. Chandrakar, J. Phys. D **11**, 1809 (1978); J. W. Denneman, *ibid.* **23**, 293 (1990).
[6]S. V. Singh, J. Appl. Phys. **103**, 083303 (2008).
[7]S. V. Singh, Ph.D. thesis, Ruhr University Bochum, 2005.
[8]I. M. El-Fayoumi and I. R. Jones, Plasma Sources Sci. Technol. **7**, 162 (1998); **7**, 179 (1998).
[9]P. A. Miller, G. A. Hebner, K. E. Greenberg, P. D. Pochan, and B. P. Aragon, J. Res. Natl. Inst. Stand. Technol. **100**, 427 (1995); J. K. Olthoff and K. E. Greenberg, *ibid.* **100**, 327 (1995).
[10]A. Schwabedissen, E. C. Benck, and J. R. Roberts, Phys. Rev. E **55**, 3450 (1997).
[11]M. A. Sobolewski and J. H. Kim, J. Appl. Phys. **102**, 113302 (2007).
[12]C. M. O. Mahony, P. D. Maguire, and W. G. Graham, Plasma Sources Sci. Technol. **14**, S60 (2005); W. G. Graham, C. M. O. Mahony, and P. G. Steen, Vacuum **56**, 3 (2000).
[13]M. Edamura and E. C. Benck, J. Vac. Sci. Technol. A **22**, 293 (2004).
[14]V. A. Godyak, R. B. Piejak, and B. M. Alexandrovich, J. Appl. Phys. **85**, 703 (1999).
[15]V. A. Godyak, R. B. Piejak, and B. M. Alexandrovich, Plasma Sources Sci. Technol. **3**, 169 (1994); R. B. Piejak, V. A. Godyak, and B. M. Alexandrovich, *ibid.* **1**, 179 (1992).
[16]I. M. El-Fayoumi, I. R. Jones, and M. M. Turner, J. Phys. D **31**, 3082 (1998).
[17]S. Xu, K. N. Ostrikov, Y. Li, E. L. Tsakadze, and I. R. Jones, Phys. Plasmas **8**, 2549 (2001).
[18]S. Xu, K. N. Ostrikov, W. Luo, and S. Lee, J. Vac. Sci. Technol. A **18**, 2185 (2000).
[19]M. A. Liberman and A. J. Lichtenberg, *Principles of Plasma Discharges and Materials Processing* (Wiley, New York, 1994).
[20]Yu. P. Raizer, M. N. Schneider, and N. A. Yatsenko, *Radio-Frequency Capacitive Discharges* (CRC, London, 1995).
[21]U. Kortshagen, I. Pukropski, and L. D. Tsendin, Phys. Rev. E **51**, 6063 (1995).
[22]V. A. Godyak, R. B. Piejak, and B. M. Alexandrovich, Plasma Sources Sci. Technol. **11**, 525 (2002).
[23]S. V. Singh, Yu. Ivanov, and H. Soltwisch, Czech. J. Phys. **52**, 576 (2002).
[24]C. W. Chung and H. Y. Chang, Appl. Phys. Lett. **80**, 1725 (2002).
[25]G. Cunge, B. Crowley, D. Vender, and M. M. Turner, Plasma Sources Sci. Technol. **8**, 576 (1999).
[26]S. V. Singh, P. Kempkes, and H. Soltwisch, Appl. Phys. Lett. **89**, 161501 (2006).
[27]V. A. Godyak and R. B. Piejak, Phys. Rev. Lett. **65**, 996 (1990).
[28]J. Cooper, J. Nucl. Energy, Part C **5**, 285 (1963).
[29]T. J. Gallagher and A. J. Pearmain, *High Voltage Measurement, Testing and Design* (Wiley, New York, 1983).
[30]R. R. J. Gagne and A. Cantin, J. Appl. Phys. **43**, 2639 (1972); P. Scheubert, U. Fantz, P. Awakowicz, and H. Paulin, *ibid.* **90**, 587 (2001).
[31]M. J. Druyvesteyn, Z. Phys. **64**, 781 (1930).
[32]S.-H. Seo, C. W. Chung, and H.-Y. Chang, Surf. Coat. Technol. **131**, 1 (2000).
[33]V. A. Godyak and V. I. Kolobov, Phys. Rev. Lett. **81**, 369 (1998).
[34]T. Kimura and K. Ohe, J. Appl. Phys. **89**, 4240 (2001).
[35]R. H. Cohen and T. D. Rognlien, Plasma Sources Sci. Technol. **5**, 442 (1996).
[36]K. N. Ostrikov, S. Xu, and M. Y. Yu, J. Appl. Phys. **88**, 2268 (2000).
[37]P. Chabert, J.-L. Raimbault, P. Levif, J.-M. Rax, and M. A. Lieberman, Phys. Rev. Lett. **95**, 205001 (2005), and references therein.
[38]M. M. Turner, D. A. W. Hutchinson, R. A. Doyle, and M. B. Hopkins, Phys. Rev. Lett. **76**, 2069 (1996), and references therein.